THE ASTROPHYSICAL JOURNAL, 492:390–401, 1998 January 1

MAGNETIC SOURCES OF THE SOLAR IRRADIANCE CYCLE

J. L. LEAN AND J. COOK
E. O. Hulburt Center for Space Research, Naval Research Laboratory, Washington, DC 20375;
lean@demeter.nrl.navy.mil, cook@hrts.nrl.navy.mil

W. MARQUETTE AND A. JOHANNESSON
Big Bear Solar Observatory, California Institute of Technology, Pasadena, CA 91125;
whm@suncub.bbso.caltech.edu, anders@suncub.bbso.caltech.edu
Received 1996 December 6; accepted 1997 August 6

ABSTRACT

Using recently processed Ca K filtergrams, recorded with a 1 Å filter at the Big Bear Solar Observatory (BBSO), we quantitatively assess the component of solar irradiance variability attributable to bright magnetic features on the Sun's disk. The Ca K filtergrams, "flattened" by removing instrumental effects and center-to-limb variations, provide information about bright sources of irradiance variability associated with magnetic activity in both active regions and dispersed active region remnants broadly distributed in the supergranule network (termed collectively "faculae"). Procedures are developed to construct both total and UV spectral solar irradiance variations explicitly from the processed Ca K filtergrams, independently of direct irradiance observations. The disk-integrated bolometric and UV facular brightness signals determined from the filtergrams between late 1991 and mid-1995 are compared with concurrent solar irradiance measurements made by high-precision solar radiometers on the *Upper Atmosphere Research Satellite* (*UARS*). The comparisons suggest that active-region and active-network changes can account for the measured variations. This good agreement during a period covering most of the decline in solar activity from the cycle 22 maximum to the impending solar minimum directly implicates magnetic features as the sources of the 11 yr irradiance cycle, apparently obviating the need for an additional component other than spots or faculae.

Subject headings: Sun: activity — Sun: faculae, plages — Sun: fundamental parameters — Sun: magnetic fields

1. INTRODUCTION

Changing magnetic activity modifies the Sun's radiative output at all wavelengths. Total (spectrally integrated) irradiance, emitted primarily from the photosphere, is about 0.1% brighter when solar activity is high during the 11 yr cycle, as in 1980 and 1990, relative to the minimum activity level of 1986 (Wilson & Hudson 1988, 1991; Foukal & Lean 1988). Larger 11 yr cycle variations occur in the Sun's short-wavelength spectrum. Ultraviolet (UV) radiation near 200 nm, emitted from the middle photosphere (Vernazza, Avrett, & Loeser 1976), varies by about 8% (Lean et al. 1998), while variations of more than a factor of 2 can occur in extreme ultraviolet (EUV) radiation at wavelengths shortward of 120 nm (Lean 1991), emitted from the upper chromosphere and transition regions.

The fact that the so-called solar constant (i.e., total radiative output) is not actually constant raises the possibility of a direct solar radiative influence on terrestrial climate (National Research Council 1994). Changes in the visible and near-infrared radiation that dominates solar total radiative output potentially impact the Earth's surface temperature and the biosphere. UV radiation creates and maintains the atmospheric ozone layer while the more substantial EUV irradiance variations affect significantly the thermodynamics of the upper atmosphere and ionosphere, contributing to space weather (National Space Weather Program 1995). Investigating potential longer term Sun-Earth connections relevant to global change and space weather requires knowledge of solar irradiance changes in the past and estimates of plausible irradiance changes in the future (Lean & Rind 1996). This motivates the development of a reliable understanding of the sources of radiative output variability in the contemporary space-borne solar monitors (National Research Council 1995).

A complete definition of the sources of the solar irradiance cycle from extant data has proved difficult, and remains ambiguous. The variations arise in part from the changing presence on the Sun's Earth-facing disk of magnetic features—dark sunspots and bright faculae in active regions and the surrounding network—which occur frequently during times of high solar activity but may be absent for days during solar mimimum conditions. Dark sunspots reduce the local radiative output of the Sun's surface, whereas photospheric faculae and chromospheric plages and network are regions of enhanced visible and UV emission, respectively (Cook, Brueckner, & VanHoosier 1980; Willson 1982; Lean et al. 1982; Foukal & Lean 1986). Variability on timescales of the Sun's rotational modulation (approximately once every 27 days) is almost wholly attributable to these effects (Willson et al. 1981; Hudson et al. 1982; Foukal & Lean 1986; Lean 1991). But whether brightness changes in magnetic features alone are the only sources needed to account for the 11 yr solar irradiance cycle, or whether nonfacular—possibly global—mechanisms are also occurring, is under debate.

An apparent missing brightness component is the basis of this debate. Calculations of the irradiance changes during the 11 yr cycle associated with sunspots and facular emission from active regions (alone), estimated by the National Oceanographic and Atmospheric Administration World Data Center (NOAA/WDC) scalings of Ca K plage areas, underestimate the observed solar cycle irradiance modulation by roughly a factor of 2 (Lean 1991). This deficit is apparent in total radiative output (Foukal & Lean 1988;

Willson & Hudson 1988; Kuhn, Libbrecht, & Dickie 1988) and in the spectrum variations at UV and EUV wavelengths (Lean 1988; 1990). Other studies (e.g., Willson & Hudson 1991; Fröhlich 1994) have pointed to the apparent inability of ground-based proxies for full-disk facular emission—specifically the 10.7 cm radio flux, the He 1083 nm equivalent width (Harvey & Livingston 1994) and the Mg core-to-wing ratio (Heath & Schlesinger 1986; DeLand & Cebula 1993; de Toma et al. 1997)—to account fully for the total irradiance brightness increase inferred from the Active Cavity Radiometer Irradiance Monitor (ACRIM) and *Nimbus* 7 space-based radiometer measurements (after correcting for sunspot influences) during maximum activity epochs.

In pointing out this deficit in the context of UV irradiance variations, Skumanich et al. (1984) suggest that the source of the missing brightness is "active" network—bright, small-scale magnetic facular features produced by active region decay that are eventually incorporated in the quiet Sun network and not tallied in the WDC scaling of the compact Ca K plage regions. This interpretation is consistent with the observation that the WDC scalings miss a significant fraction of bright Ca K emission on the solar disk. Analysis of Mount Wilson Observatory spectroheliograms indicates that near-maximum epochs of the activity cycle, about 20% of the Sun's disk is covered with bright Ca K emission at intensity levels at least 3 times that of the quiet Sun (Sheeley 1967). This is a factor of 2 larger than the WDC plage areas on the same days (Lean 1988). Attempts to quantify the contribution to irradiance variability of all bright magnetic sources on the Sun's disk have utilized a variety of facular surrogates. Detailed analyses of magnetograms (Foukal, Harvey, & Hill 1991; Lawrence, Chapman, & Walton 1991) and visible light images (Nishikawa 1990) suggest that additional smaller-scale magnetic features do indeed contribute significant brightness to the global irradiance signal, but none of these studies has yet replicated the entire amplitude and detailed temporal structure of the observed solar irradiance cycle.

Certain studies based on solar limb photometry suggest, instead, that the missing brightness component is of nonfacular origin, possibly a global mechanism such as a few degrees change in the Sun's surface temperature (Kuhn, Libbrecht, & Dicke 1988; Willson & Hudson 1991). Such a changing photospheric temperature also provides a plausible explanation for solar cycle variations in helioseismic splitting coefficients and mode centroid frequencies (Kuhn 1989). While a small change in photospheric temperature is probably indistinguishable from unresolved flux excess in active network, Kuhn & Libbrecht (1991) argue that the missing component is nonfacular because it appears to lack the significant limb brightening evident in active region visible light faculae.

Ground-based full-disk Ca K filtergrams permit quantitative determination of the intensity distribution of bright magnetic sources on the Sun. Ca K images made at BBSO have been newly processed for the period from 1987 to 1996 (Johannesson, Marquette, & Zirin 1995, 1997), which covers present-day space-based irradiance monitoring by ACRIM and the Solar Stellar Irradiance Comparison Experiment (SOLSTICE) with unprecedented long-term repeatability on board the *UARS*. We develop general procedures to construct solar radiative output variability by utilizing enhanced emission in Ca K filtergrams as a proxy for magnetic brightness sources present on the Sun's disk, including active regions and active network. Specific calculations made for the total and UV radiation at 200 nm are compared with direct observations of the variations measured independently by the *UARS* solar radiometers since 1991 September. These comparisons permit quantitative assessment of magnetic sources of irradiance variability at the Sun's surface and in the middle photosphere during most of the decline in solar activity, from near-maximum levels of solar cycle 22 to the impending solar minimum.

2. SOLAR IRRADIANCE AND IMAGE DATA DURING SOLAR CYCLE 22

2.1. *Total Irradiance*

The ACRIM II measurements on the *UARS* contribute to a 17 yr record of solar total irradiance, shown in Figure 1, that includes earlier measurements made by the ACRIM I radiometer on the *Solar Maximum Mission* (*SMM*) spacecraft (Willson & Hudson 1991; Willson 1994) and by radiometers on the *Nimbus* 7 spacecraft (Hickey et al. 1988; Hoyt et al. 1992; Kyle et al. 1993) and the *Earth Radiation Budget Satellite* (*ERBS*) (Lee et al. 1995). ACRIM comprises three self-calibrating, dual cavity pyrheliometers each of which measures the Sun's total radiation (without wavelength discrimination) on different duty cycles by comparing incoming solar and electrically generated power. The different duty cycles ensure different rates of in-flight sensitivity degradation which are removed from the measured signals to determine the actual changes in solar radiation with a long-term repeatability goal of a few hundredths percent (Willson 1979, 1984).

Differences exist among the absolute radiometric scales of different space-based radiometers, and cause the offsets of the various measurements from each other, evident in Figure 1. We add 1.65 W m^{-2} to the reported ACRIM II irradiance data in Figure 1 to place it on the ACRIM I irradiance scale. With this adjustment, ACRIM II total irradiance values near the end of 1995 approach the level of the quiet Sun determined by ACRIM I in 1986. We adopt this adjustment in lieu of using either the *Nimbus 7 or ERBS* data to cross-calibrate ACRIM I and ACRIM II, because drifts in the radiometer sensitivities with time contribute significant uncertainties in this cross-calibration (Fröhlich 1994; Mecherikunnel 1994; Kyle et al. 1993, Lee et al. 1995).

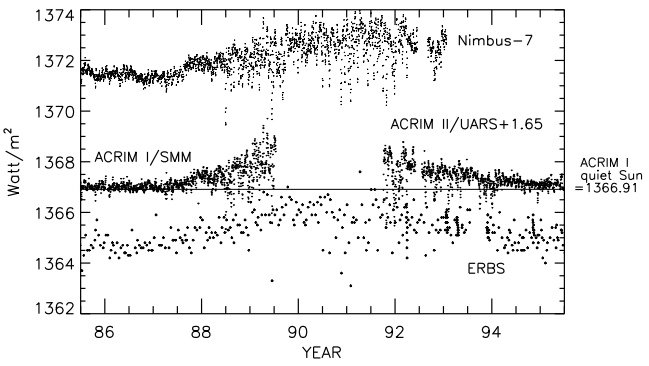

FIG. 1.—Observations by space-based radiometers of the Sun's total irradiance during cycle 22. The thin line is the level of the quiet-Sun irradiance appropriate for ACRIM I data. ACRIM II measurements are adjusted upward to the ACRIM I scale by adding 1.65 W m^{-2}, so that the ACRIM II data in 1995 are consistent with the quiet-Sun level.

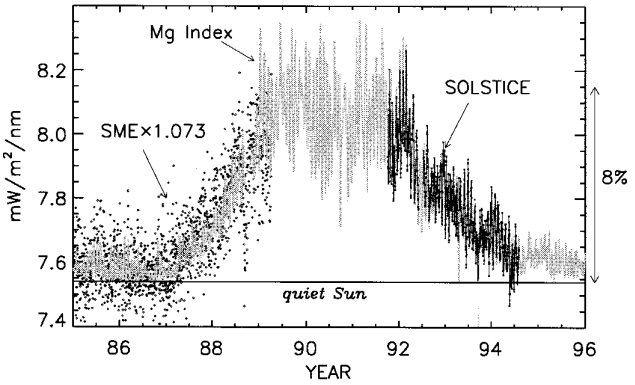

FIG. 2.—Measurements of the Sun's 200 nm irradiance in solar cycle 22 made by SOLSTICE on *UARS* (*small asterisks connected with thin line*) since late 1991 and by the *SME* (*small diamonds*) prior to that. The *SME* data have been adjusted upward by 7.3% by using a linear regression of the Mg index (*gray line*) with the SOLSTICE data for cross-calibration. A quiet-Sun irradiance of 7.54 mW m^{-2} nm^{-1} is consistent with both SOLSTICE and adjusted *SME* data.

Although our adopted adjustment for the ACRIM II irradiance scale is consistent with the ACRIM I–ACRIM II offset of 1.8 ± 0.6 W m^{-2} based on the overlapping *ERBS* measurements, it does not support the 2.5 ± 0.6 W m^{-2} adjustment implied by the *Nimbus* 7 data. Recent studies by Lee et al. (1995) and Chapman, Cookson, & Dobias (1996) have identified inconsistencies of 0.4–0.8 W m^{-2} in the *Nimbus* 7 data since 1989 that are the probable cause of this discrepancy. A more reliable estimate of the Sun's quiet total irradiance during solar cycle 22 awaits future measurements by ACRIM II during the 1996 epoch.

2.2. *Ultraviolet Irradiance*

Also on board the *UARS*, SOLSTICE records the UV irradiance at wavelengths from 120 to 420 nm emitted from throughout the Sun's photosphere and chromosphere. SOLSTICE spectrally disperses and detects incident solar UV radiation by using gratings and photomultipliers. Periodic comparisons of the Sun's signal with an average signal from a set of bright blue stars provides inflight radiometric tracking with a long-term repeatability goal of $\pm$ 1% (Rottman, Woods, & Sparn 1993; Woods, Rottman, & Ucker 1993). The SOLSTICE solar UV spectral irradiance measurements on *UARS* are considered the most accurate and repeatable to date, having undergone extensive preflight characterization and calibration, in-flight sensitivity tracking, and cross-validation (Woods et al. 1996). Figure 2 compares irradiance observations made by SOLSTICE at 200 nm (Version 8) during the descending phase of solar cycle 22 with the *Solar Mesosphere Explorer* (*SME*) observations during the early part of the solar cycle (Rottman 1988). Lacking overlap of the *UARS* and *SME* measurements, the Mg index proxy provides cross-calibration of the two data sets, requiring a 7.3% increase in *SME* data relative to the *UARS* 200 nm scale. Aside from their absolute calibration differences, the SOLSTICE *UARS* and *SME* data provide mutually consistent indications of a 200 nm 11 yr irradiance cycle of amplitude 8% and a quiet-Sun level (See Fig. 2) of 7.54 mW m^{-2} nm^{-1}.

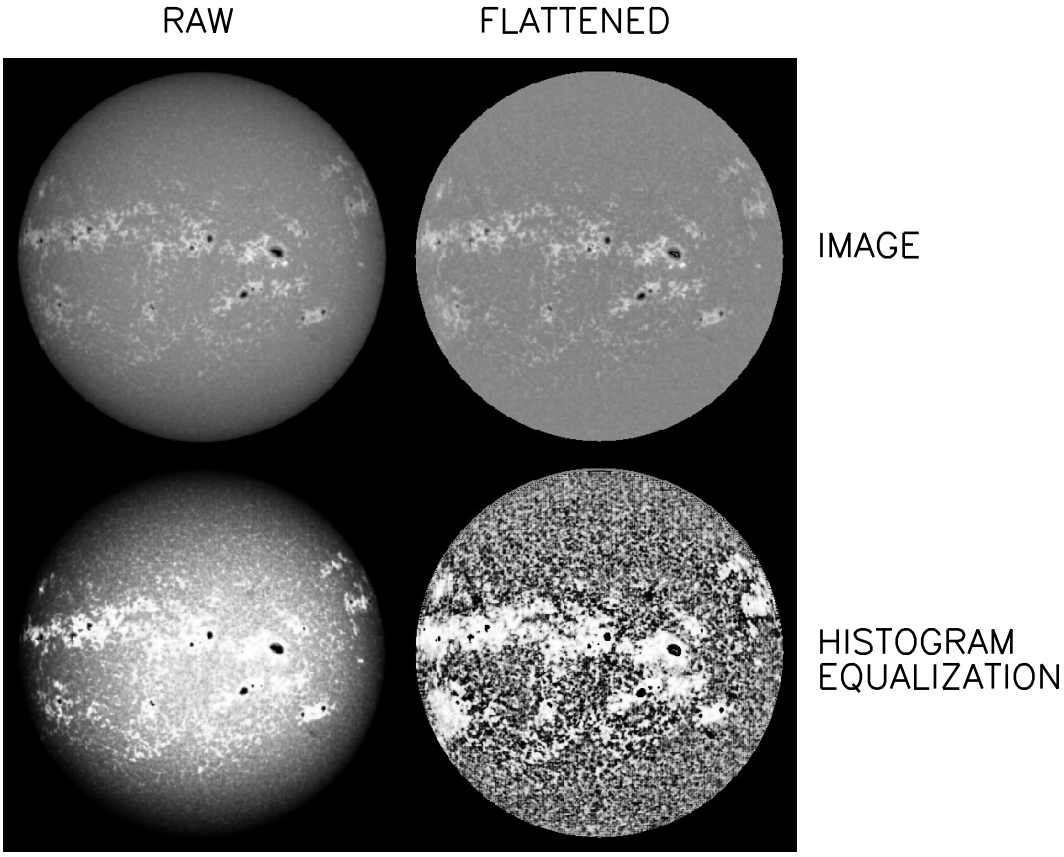

FIG. 3.—The raw BBSO Ca K image (*upper left panel*) 1992 January 31 is compared with the "flattened" image (*upper right panel*), after removal of larger scale instrumental effects and the center-to-limb variation. Histogram equalizations of the images (*bottom panels*) amplify their details for visual inspection.

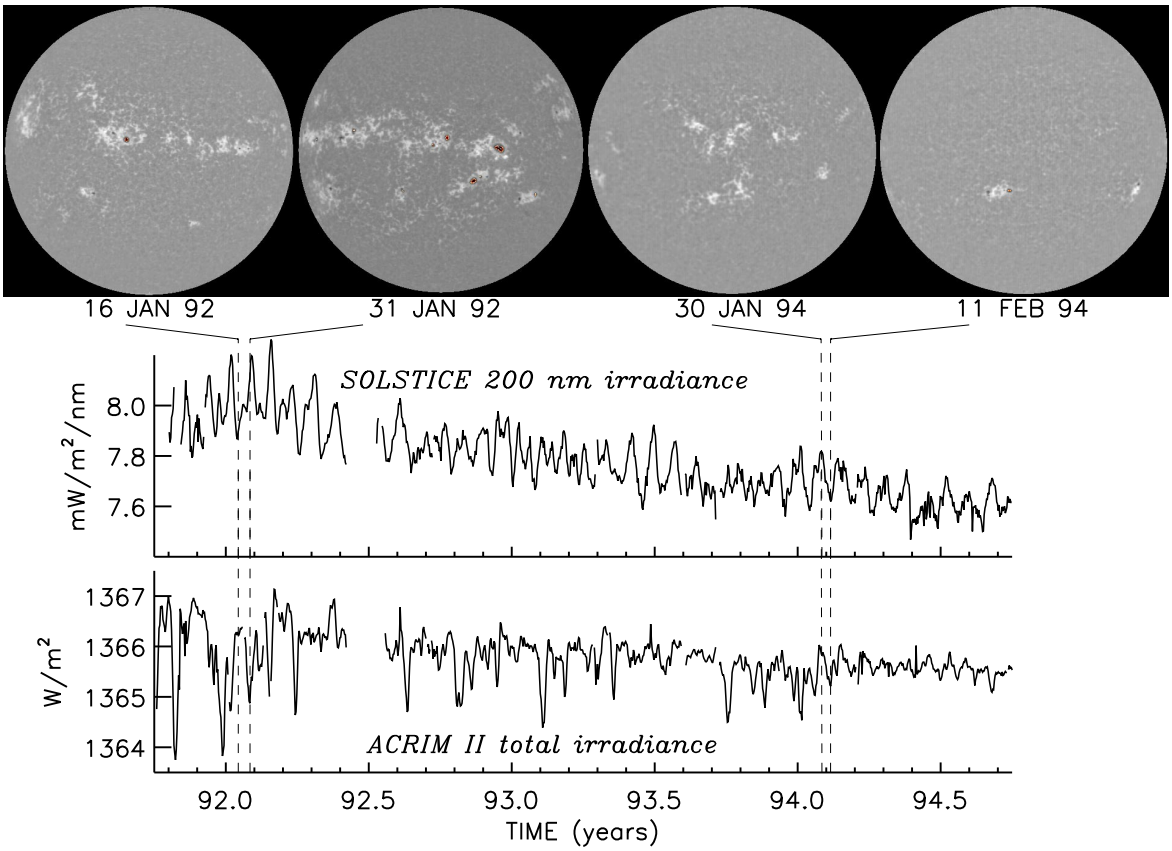

FIG. 4.—Inhomogeneous distribution of bright emission on the solar disk recorded by Ca K filtergrams throughout the declining phase of solar cycle 22, concurrent with UV and total irradiance monitoring by, respectively, SOLSTICE and ACRIM II on *UARS*.

Our adopted quiet-Sun level for the 200 nm irradiance is consistent with the lowest levels of irradiance during solar minimum conditions in 1986 implied by the Mg index proxy data scaled to the SOLSTICE fluxes.

2.3. *Ca K Images*

Daily K-line images of the Sun have been obtained over the past decade at the BBSO using a 1 Å Daystar filter to spectrally isolate the core of the UV Fraunhofer Ca II K line at 393 nm, with a prime goal of elucidating magnetic flux evolution and morphology on the solar disk (Zirin 1974). Actual pixel values of these digitized video images range from 0 to 255 and are linearly related to the Ca K line emission from the solar disk. Recent processing renders these filtergrams applicable for the more stringent application of quantitative radiometric studies (Johannesson et al. 1995, 1997). Figure 3 illustrates the results of the Ca K image processing that involves careful removal of instrumental effects in the images and, at the same time, the center-to-limb variations, to produce residual "flattened" images of enhanced Ca K emission relative to the background Sun. The images are processed further to determine their centers and radii.

Ca K images processed in this manner provide quantitative information about enhanced emission from magnetic regions on the Sun, relative to the background emission and independently of the Ca II limb darkening. Remaining after removing global scale inhomogeneities in the background emission—as revealed by the histogram equalization of the raw Ca K images in Figure 3—are compact active regions, the Ca K plages, and smaller scale phenomena which compose the active and quiet network. The flattened Ca K images in Figure 4 demonstrate the changing surface morphology of these features concurrent with the measured total and UV irradiances as solar activity decreased during cycle 22.

3. CONSTRUCTION OF IRRADIANCE VARIABILITY FROM MAGNETIC SOURCES

During times of solar minima, in the absence of activity-related features on its disk, the Sun's "quiet" radiation $F_Q(\lambda)$ at wavelength λ reaching the Earth (at a distance from the Sun of 215 times the solar radius) is

$$F_Q(\lambda) = \frac{2\pi I_Q(\lambda, 1) \int R(\lambda, \mu)\mu \, d\mu}{(215)^2} . \quad (1)$$

This expression integrates the specific intensity $I_Q(\lambda, 1)$ at the center of the solar disk ($\mu = 1$) over the entire disk using the center-to-limb function $R(\lambda, \mu)$ to define the ratio of $I(\lambda, \mu)/I(\lambda, 1)$ at heliocentric position μ which ranges from 0 to 1 (Cook, Brueckner, & VanHoosier 1980; Lean et al. 1982). Table 1 provides examples of the parameters in equation (1) for bolometric (i.e., spectrally integrated) and 200 nm radiation.

The quiet Sun defined in equation (1) is itself a mix of elements of different brightness that comprise the centers

TABLE 1

AVERAGE PROPERTIES OF SUN'S BOLOMETRIC AND 200 NANOMETER RADIATIVE OUTPUT

PARAMETER			
Symbol	Definition	BOLOMETRIC	UV 200 nm
F_Q	Quiet-Sun irradiance	1366.91 W m^{-2} ACRIM I 1365.26 W m^{-2} ACRIM II	7.54 mW m^{-2} nm^{-1} SOLSTICE
$R(\mu)$	Center-to-limb function	$(3\mu + 2)/5$	$p + q\mu + r\mu^2 + s\mu^3 + t\mu^4$ $p = 0.3$ $q = 0.055$ $r = 2.15$ $s = -3.32$ $t = 1.8$
$\int R(\mu)\mu\, d\mu$.....	Center-to-limb-integral	0.4	0.3446
C_F	Facular residual intensity contrast conversion from Ca K intensity (1992 January 31)	$(a + bI_{\mathrm{Ca\,K}})$ $\times (c + d\mu + e\mu^2 + f\mu^3 + g\mu^4 + h\mu^5)$ $a = 0.96$ $b = 0.00031$ $c = 1.0137$ $d = 0.057$ $e = -0.123$ $f = -0.103$ $g = 0.28$ $h = -0.125$	$a + bI_{\mathrm{Ca\,K}}$ $a = -2.133$ $b = 0.02451$
	Facular residual intensity contrast for Ca K pixel intensity $I_{\mathrm{Ca\,K}} = 170$ at disk center ($\mu = 1$)	0.013	1.04

NOTE.—Quiet-Sun irradiances, deduced from space-based irradiance measurements, are identified in Figs (1) and 2, respectively. The quiet-Sun irradiance of 1365.26 W m^{-2} on the ACRIM II calibration scale is equivalent to 1366.91 W m^{-2} on the ACRIM I scale based on the adopted cross-calibration of 1.65 W m^{-2}. Center-to-limb functions for bolometric radiation are from Allen 1981 and for UV radiation at 200 nm are from Samain 1979.

and boundaries of cells identified as the chromospheric network in Ca K images (Skumanich, Smythe, & Frazier 1975; Skumanich et al. 1984). This quiet network is evident during times when large-scale solar magnetic features are absent from the disk surface, as on certain days during solar minima, but it may nevertheless change over timescales longer than the 11 yr cycle (Skumanich et al. 1984; White, Skumanich, Lean, Livingston, & Keil 1992), and these changes are not addressed here.

Magnetic features—dark sunspots, bright visible-light faculae, UV plages, and dispersed magnetic remnants—are typically present on the Sun's disk, especially during times of high activity, when they occur frequently. Depending on their areas, locations, and local fluxes relative to the background Sun, these features alter the otherwise homogeneous distribution of the quiet-disk emission, so that the net solar radiative output is

$$F(\lambda) = \frac{2\pi I_Q(\lambda, 1) \int C(\lambda, \mu) R(\lambda, \mu)\mu\, d\mu}{(215)^2}, \qquad (2)$$

where $C(\lambda, \mu) = I(\lambda, \mu)/I_Q(\lambda, \mu)$ is the ratio of the Sun's radiance at heliocentric location μ relative to the surrounding quiet photosphere. Separating radiance elements on the solar disk into those that are darker and brighter than the quiet Sun permits the rearrangements of equation (2):

$$F(\lambda) = F_Q(\lambda) + \frac{2\pi I_Q(\lambda, 1)}{215^2} \int [C_s(\lambda, \mu) - 1] R(\lambda, \mu)\mu\, d\mu + \frac{2\pi I_Q(\lambda, 1)}{215^2} \int [C_F(\lambda, \mu) - 1] R(\lambda, \mu)\mu\, d\mu \qquad (3)$$

where $C_s(\lambda, \mu) - 1$ and $C_F(\lambda, \mu) - 1$ are the residual intensity contrasts of the darker and brighter elements, respectively sunspots and faculae.

The disk-integrated flux determined from an image of the Sun is likewise calculated by summing over all elements of the image that are respectively darker and brighter than the background quiet Sun. Denoting $\Delta F_S(\lambda)$ and $\Delta F_F(\lambda)$ as the radiative changes attributable to spot and facular elements in a solar image, then

$$F(\lambda) = F_Q(\lambda) + \sum_{i=1}^{N_{\mathrm{SPOT}}} \Delta F_S(\lambda) + \sum_{j=1}^{N_{\mathrm{FAC}}} \Delta F_F(\lambda)\,. \qquad (4)$$

Ground-based white-light and Ca K images of the Sun provide data to numerically reconstruct the influences of sunspots and faculae on solar radiative output. Figure 4 illustrates this quantitatively. As solar activity decreases from 1992 to 1994, there is an overall long-term decline in both the UV and total irradiance concurrent with the reduction of bright features—active region and network faculae—on the Sun's disk. Superimposed on this overall downward trend is a significant rotational modulation arising primarily from the changing distribution of the active regions on the disk. The rotational modulation amplitude is strongest during times of high solar activity as during early 1992, near the maximum of cycle 22, when both notable sunspots and faculae are present on the Sun's disk. From 1992 January 16 to January 31 there is a net decrease in total irradiance because of the increase in radiation blocking by sunspots on the disk. At the visible wavelengths that dominate the total radiative output the accompanying increase in bright magnetic features has insufficient flux to counter this sunspot-related decrease.

However, the 200 nm irradiance increases over the same period because faculae are much brighter relative to sunspots at shorter wavelengths than at visible wavelengths. A different scenario occurs from 1994 January 30 to February 11 when overall solar activity is lower. In the absence of sunspots, rotational modulation is associated with faculae emission alone, and causes both the total and UV radiation to decrease in direct response to the reduction of bright emission sources on the disk over this period.

3.1. *Sunspot Darkening*

Foukal (1981) and Fröhlich, Pap, & Hudson (1994) estimate the change in radiation, $\Delta F(\lambda)_S$, at wavelength λ, attributable to a sunspot of actual area A at heliocentric position μ on the solar disk relative to the background disk-integrated radiation, $F_Q(\lambda)$, as

$$\frac{\Delta F_S(\lambda)}{F_Q(\lambda)} = \frac{5\mu A_{\rm WDC}[C_S(\lambda) - 1]R(\lambda, \mu)}{2}, \quad (5)$$

where $A_{\rm WDC} = A/(2\pi R_\odot^2)$ is the sunspot area in units of the solar hemisphere (as given in the NOAA World Data Center records) and $R_\odot$ is the solar radius. The residual intensity contrast of the sunspot, $C_S(\lambda) - 1 = I_S(\lambda)/I(\lambda) - 1$, is the ratio of the flux deficit in the spot, $I_S(\lambda) - I(\lambda)$, relative to that from the background solar photosphere $I(\lambda)$. Equation (5) assumes that $C_S(\lambda)$ is the same at different positions on the solar disk (i.e., invariant with respect to μ; Allen 1981). As in earlier equations, $R(\lambda, \mu)$ is the center-to-limb function.

For bolometric (i.e., spectrally integrated) radiation with $R^{\rm BOL}(\mu) = (3\mu + 2)/5$ and denoting $S = \int F(\lambda)d\lambda$, equation (5) reduces to

$$\frac{\Delta S_S}{S_Q} = \frac{\mu A_{\rm WDC}(C_S - 1)(3\mu + 2)}{2}. \quad (6)$$

Summing equation (6) over all sunspots present on the disk using $C_S - 1 = -0.3235$ (Allen 1981) yields the so-called bolometric sunspot blocking function, P_S (Foukal 1981), also called the photometric sunspot index (Hudson et al. 1982; Chapman & Meyer 1986). Recent studies provide empirical evidence for the dependence of sunspot residual intensity contrast on sunspot area, in the sense that larger sunspots are darker than smaller spots. According to Brandt, Stix, & Weinhardt (1994),

$$C_S - 1 = -[0.2231 + 0.0244 \log_{10}(A_{\rm WDC})]. \quad (7)$$

Figure 5 documents the bolometric energy changes attributable to the net sunspot darkening in 1992, obtained by summing equation (6) over all sunpots on the disk using information about sunspot areas and locations archived by the NOAA World Data Center from multiple daily ground-based white-light images, and utilizing equation (7) to specify their residual intensity contrasts.

At different wavelengths, the contrast of a sunspot differs from its bolometric counterpart, altering the net radiative output influence of sunspot darkening relative to that of facular brightening. At 200 nm, for example, although sunspots are evident in images of the Sun, their net influence on the disk-integrated modulation is negligible compared with that of bright faculae whose contrast is enhanced significantly relative to bolometric values. The time series in Figure 4 illustrate the increase in the Sun's radiation at 200 nm as facular coverage of the disk increases from 1992 16–31 Jan, even in the presence of significant sunspots. Sunspot influences on UV radiative output begin to be discernible only at wavelengths longward of 250 nm (Lean et al. 1998).

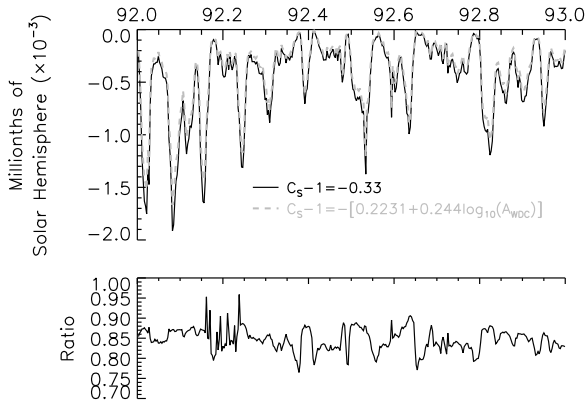

FIG. 5.—Two different determinations of sunspot darkening in 1992 are compared in the upper panel using, respectively, constant (*solid line*) and area-dependant (*gray dashed line*) bolometric spot contrast functions. The lower panel shows the ratios of the two curves in the upper panel.

3.2. *Facular Brightening*

An approach analogous to equation (5) estimates the change in radiation, $\Delta F(\lambda)_F$, attributable to a bright magnetic element (i.e., faculae in large, dense active regions or in the more dispersed active network) on the solar disk (Foukal 1981; Foukal et al. 1991) as

$$\frac{\Delta F_F(\lambda)}{F_Q(\lambda)} = \frac{5\mu\, A_F[C_F(\lambda, \mu) - 1]R(\lambda, \mu)}{2}, \quad (8)$$

where A_F is the area of the facular element in units of the solar hemisphere, $C_F(\lambda, \mu) - 1$ is the element's residual intensity contrast, and $R(\lambda, \mu)$ is the center-to-limb function. The contrast of faculae, unlike that of sunspots, depends strongly on μ, and this dependence varies with wavelength. At visible wavelengths, faculae are brighter toward the limb than at disk center, but the functional form of this center-to-limb variation remains poorly defined and is a major source of uncertainty in the evaluation of equation (8). Figure 6*a* shows two scenarios adopted to evaluate equation (8) for bolometric radiation in which facular contrast maximizes prior to the limb (*A*), consistent with the results of Libbrecht & Kuhn (1985), versus at the limb (B), as indicated by Lawrence (1988). Figure 6*b* compares $R(\lambda, \mu)$ for $\lambda =$ 200 nm with the bolometric limb darkening $R^{\rm BOL}(\mu) = (3\mu + 2)/5$.

Uncertainties in A_F and $C_F(\lambda, \mu) - 1$ in equation (8) for faculae are significantly larger than in A_S and $C_S(\lambda) - 1$ in the analogous equation (5) for sunspots. Observational determination of the areas and contrasts of even the largest, most dense active region faculae are significantly less reliable than for sunspots. Compared with the compact dark sunspots, bright magnetic elements are more dispersed on the solar disk and, at visible wavelengths, have much lower bolometric contrasts (a few percent vs. 30%). Some specific studies have used Ca K solar images to identify the larger, more compact faculae associated with prominent active regions by their much brighter chromospheric extensions (Vršnak, Placko, & Ruzdjak 1991; Steinegger, Brandt, & Haupt 1996). But magnetic activity also produces smaller

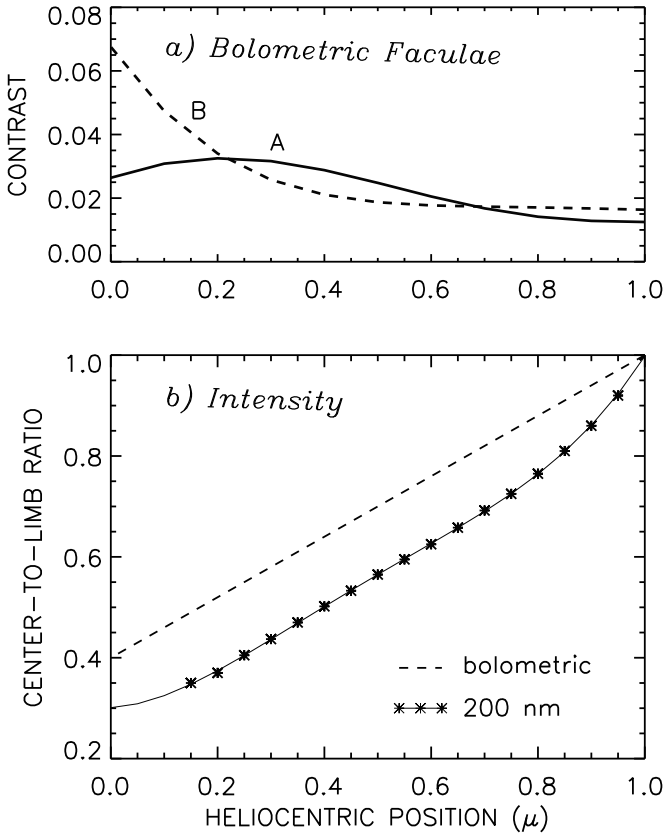

FIG. 6.—(*a*) Two different representations of the center-to-limb dependence of the bolometric residual intensity contrast. Curve A is consistent with Libbrecht & Kuhn (1985), while curve B reflects the behavior identified by Lawrence (1988). (*b*) Center-to-limb functions for bolometric (Allen 1981) and 200 nm specific intensity (Samain 1979). Both the residual intensity contrast of bolometric faculae and the specific intensity of bolometric and UV radiation depend on the location of the emitting region of the Sun's disk.

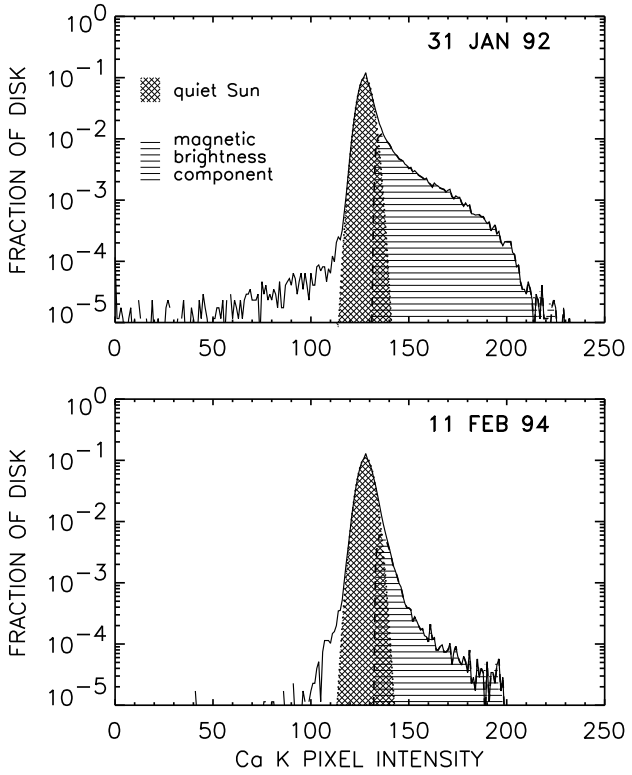

FIG. 7.—Histograms of the distribution of emission in the "flattened" Ca K filtergrams quantify changes in the number of emitting pixels at each Ca K intensity level during a period of high solar activity in cycle 22 (1992 January 31) compared with moderate to low activity (1994 February 11). Each pixel of a digitized Ca K image has a value in the range 0–255 that is linearly related to Ca K emission from the solar disk. The diagonal cross-hatched regions identify Gaussian functions fitted to the most abundant pixels of each brightness distribution. The horizontal-line hatching identifies those pixels in the high-intensity tail of the histograms that are not accounted for by the Gaussian functions and which are altered notably by the changing magnetic activity of the Sun. These pixels in the high-intensity histogram tails are adopted as surrogates for bright magnetic sources of solar irradiance. The number of pixels with intensity levels less than the Gaussian function also changes because of the presence of dark sunspots, which are likewise decreased when solar activity is low.

faculae that reside within the network of enhanced emission that covers the entire solar disk. These smaller faculae—or active network (Skumanich et al. 1984)—merge with the network that composes the background "quiet" photosphere. As a result, quantifying the active network contribution to irradiance modulation has proved extremely difficult (Nishikawa 1990; Foukal et al. 1991), and the approach has yet to be implemented adequately for determination of the global, disk-integrated facular signal present in either bolometric or spectral irradiance variability.

Enhanced Ca K emission is well recognized as occurring in regions on the Sun's disk (e.g., plages) where magnetic flux is enhanced and which are, as a result, sites of excess emission at UV wavelengths (Cook et al. 1980). Enhanced Ca K emission also occurs in the vicinity of bright faculae, formed lower in the Sun's photosphere, that contribute to total irradiance variations (Chapman & Sheeley 1968). Because of this association, full-disk Ca K images provide a methodology to quantitatively determine the influence of magnetic activity on solar irradiance. The histograms in Figure 7 of two of the flattened Ca K images in Figure 4 quantify the distribution of Ca K emission intensity over the full solar disk on 1992 January 31 (near cycle and rotational maxima) and on 1994 February 11 (during rotation minimum near cycle minimum). These histograms show the number of pixels present in the digitized Ca K images that have a specified value, ranging from 0 to 255, that is linearly related to Ca K emission from the solar disk. The histograms are assymetrical about their peaks, having larger numbers of bright pixels during times of higher solar activity (e.g., 1992 January 31), and approaching a distribution that can be approximated by a Gaussian function (indicated by the cross-hatched regions in Fig. 7) when solar activity is lower (e.g., 1994 February 11).

Magnetic activity notably affects those pixels indicated by the horizontal-line hatching in the Ca K images in Figure 7. These pixels have brightness levels in excess of a Gaussian representation of the main part of the histogram (shown by cross-hatching), and their distribution is shown with greater clarity in Figure 8 as residuals, obtained by subtracting a Gaussian function fitted to the most abundant pixels' brightnesses in the histograms in Figure 7. The residual histograms contain information about magnetic brightness sources of solar radiative output variability with which to evaluate equation (8) numerically. One facular pixel of a Ca K filtergram with a total number of $N_{\rm PIX}$ pixels on the disk has an area $A_F = 1/(2\mu N_{\rm PIX})$ in units of the solar hemisphere. From equation (8), the contribution of this one

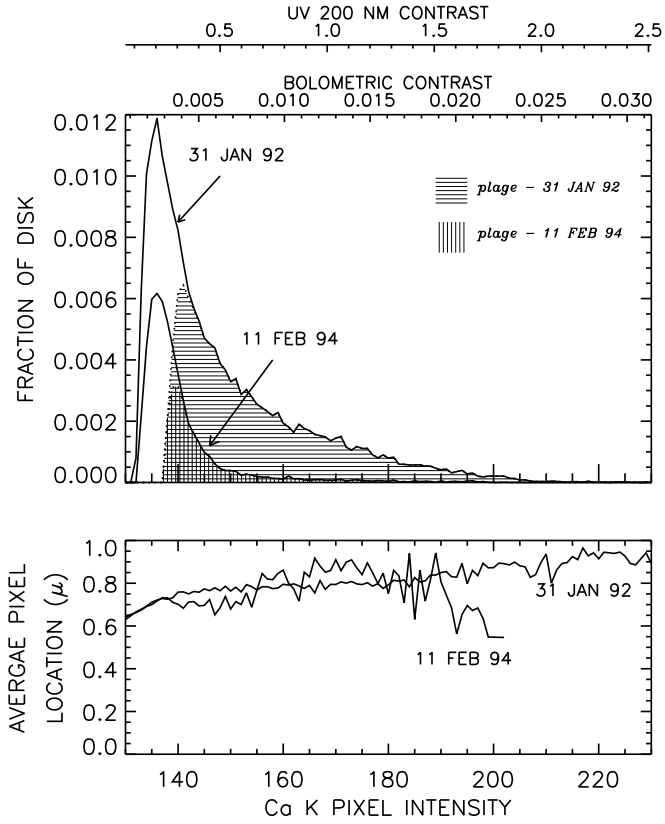

FIG. 8.—Distributions of residual magnetic flux obtained by removing from the Ca K histograms in Fig. 7 those parts of the distributions accounted for by the Gaussian functions (*upper panel*). Plages are qualitatively identified in the figure as the brightest elements of these residuals. The upper scales show conversions from Ca K brightness levels to residual intensity contrasts for both bolometric and 200 nm radiation. Mean values of the heliocentric locations of the pixels in each Ca K intensity bin are shown in the lower panel.

bright pixel to the full disk irradiance is

$$\frac{\Delta F_F(\lambda)}{F_Q(\lambda)} = \frac{5[C_F(\lambda, \mu) - 1]R(\lambda, \mu)}{4N_{\rm PIX}}, \quad (9)$$

and all such pixels in a solar image modify the radiative output by an amount

$$\frac{\sum_{j=1}^{N_{\rm FAC}} \Delta F_F(\lambda)}{F_Q(\lambda)} = \frac{5\sum_{j=1}^{N_{\rm PIX}} [C_F(\lambda, \mu_j) - 1]R(\lambda, \mu_j)}{4N_{\rm PIX}}, \quad (10)$$

where the summation is over all pixels on the disk, $N_{\rm FAC}$, attributable to magnetic sources of brightness in excess of the quiet Sun.

The residual histograms in Figure 8 provide estimates of the numbers and intensities relative to the quiet Sun of bright magnetic elements and permit further modification of equation (10) to

$$\frac{\sum_{j=1}^{N_{\rm FAC}} \Delta F_F(\lambda)}{F_Q(\lambda)} = \frac{5\sum_{k=1}^{N_{\rm BINS}} [C_F(\lambda, \bar{\mu}_k) - 1]R(\lambda, \bar{\mu}_k)N_k}{4N_{\rm PIX}}, \quad (11)$$

where N_k is the number of pixels with a given intensity in the histograms, $\bar{\mu}$ is the average heliocentric position of these pixels, and the summation is over all intensity bins of the residual histogram. Figure 8 illustrates $\bar{\mu}$ for the residual histograms on 1992 January 31 and 1994 February 11.

Evaluating equation (11) requires the conversion of Ca K intensity to the corresponding intensity of radiation at the wavelength of interest. This mapping depends on spatial resolution, since poorer resolution reduces the brightness of smaller scale features which become blended with the background quiet Sun. Lacking specific observations of the bolometric and UV contrasts corresponding to Ca K emission in the BBSO filtergrams, the relationship between the intensity ratio $C_F(\lambda, \mu)$ for radiation at wavelength λ from a pixel at location μ with Ca K intensity $I_{\rm Ca\,K}$ is assumed to be

$$C_F(\lambda, \mu) = (a + bI_{\rm Ca\,K})(c + d\mu + e\mu^2 + f\mu^3 \ldots), \quad (12)$$

in which the linear relation $a + bI_{\rm Ca\,K}$ converts Ca K emission to an equivalent intensity ratio at the wavelength of interest (Cook & Ewing 1990) and the polynomial expression accounts for the μ dependence of this intensity ratio.

Figure 8 provides numerical values for the bolometric and UV residual intensity contrasts adopted for Ca K pixels in the intensity histograms on 1992 January 31. The contrasts are consistent in a general manner with the few independent estimates available. By statistically relating the facular contribution to total irradiance variations with the intensity of the associated Ca K plages, Vršnak et al. (1991) infer bolometric plage residual intensity contrasts ranging from 0.009 to 0.024, which match closely those in Figure 8 attributed to plage regions, identified in the Ca K histograms after subtracting a Gaussian representation of active network. From observations of bright plages resolved along the slit of the NRL S082B slit spectrograph on *Skylab*, Cook et al. (1980) determine a residual intensity contrast of 1 at 200 nm, which in Figure 8 corresponds with the midrange of Ca K plage pixels present during high activity (1992 January). From balloon-borne, 200 nm filtergrams, Hersé (1979) ascribes a residual intensity contrast of 0.5 to small active regions, also consistent with the 200 nm residual intensity contrasts attributed to the range of Ca K pixel intensities in Figure 8.

4. COMPARISON OF MEASURED AND CONSTRUCTED IRRADIANCE BRIGHTNESS COMPONENTS

Equations (11) and (12) permit construction of the brightness component of radiative output directly associated with regions of enhanced magnetic flux on the Sun's disk, as identified by bright Ca K pixels. Comparison of the brightening constructed explicitly from the Ca K images with that determined observationally from space-based solar radiometry, assesses the contributions of these bright magnetic sources to solar irradiance variations. Comparisons are made for two cases—bolometric radiation that emerges from the vicinity of the Sun's visible surface and UV 200 nm radiation emitted from the middle photosphere, about 250 km above the visible surface.

4.1. *Total Irradiance*

Removing the sunspot darkening component and the bolometric quiet Sun, S_Q, from the total irradiance, S, measured by a space-based radiometer provides a radiometric determination of the bolometric brightness component as

$$\Delta S_{\rm FAC}^{\rm MEAS} = S - S_Q - S_Q \sum_{i=1}^{N_{\rm SPOTS}} \frac{\mu(3\mu + 2)}{2} \times A_{\rm WDC}[0.2231 + 0.0244 \log_{10}(A_{\rm WDC})], \quad (13)$$

where, as noted previously, the summation term defines the sunspot blocking function (specified by eqs. [6] and [7]),

and is evaluated using information about sunspot regions obtained from the WDC (Foukal & Lean 1988; Lean et al. 1998). Evaluations of equation (13) from 1991 October to 1995 June shown in Figure 9 (*gray solid line*) utilize the ACRIM II measurements of S with $S_Q = 1365.26$ W m^{-2}. Although the ACRIM II has yet to record the minimum irradiance in cycle 22, the adopted value of S_Q is consistent with the ACRIM I quiet-Sun irradiance of 1366.91 W m^{-2} measured in 1986 and the calibration offset of 1.65 W m^2 between ACRIM I and ACRIM II (see Fig. 1).

For comparison with the estimates from equation (13), the bolometric brightness component calculated directly from the residual Ca K histograms, also shown in Figure 9 (*thin line with solid circles*), is

$$\Delta S_{\rm FAC}^{\rm Ca\ K} = S_Q \sum_{k=1}^{N_{\rm BINS}} \frac{(3\bar{\mu}_k + 2)N_k}{4N_{\rm PIX}} \times [(a + bI_{\rm Ca\,K})(c + d\bar{\mu}_k + e\bar{\mu}_k^2 + f\bar{\mu}_k^3 + g\bar{\mu}_k^4) - 1] , \quad (14)$$

where the polynomial expression in $\bar{\mu}$ reproduces the limb dependence of the contrast identified as A in Figure 6*a*. Table 1 lists values of the polynomial coefficients, and provides representative values for the conversion of $I_{\rm Ca\,K}$ to disk center residual intensity contrasts.

Figure 9 demonstrates clearly that the measured and constructed bolometric brightness components track each other closely during the entire descending phase of cycle 22 (see Fig. 9*a*), as well as during solar rotation in activity maximum and minimum epochs (shown respectively in the lower panels of Fig. 9). The 779 mutual points in Figure 9*a* have a correlation coefficient of 0.9 (using contrast A in Fig. 6; for contrast B, the correlation coefficient is 0.89). The standard deviation of the measured and reconstructed brightness differences is 0.21 W m^{-2} (0.27 W m^{-2} for contrast B), which is 10% of the roughly 2 W m^{-2} decrease in bolometric brightness (see Fig. 9) that occurs during the decline of solar cycle 22.

4.2. *Ultraviolet Irradiance*

Bright facular emission dominates irradiance variations at wavelengths shorter than 200 nm because the contrast of faculae increases rapidly relative to that of the competing sunspot depletion mechanism. Thus, subtracting the background quiet Sun at 200 nm, $F_Q(200)$, from the directly measured 200 nm irradiance, $F(200)$, determines the brightness component as

$$\Delta F_{\rm FAC}^{\rm MEAS}(200) = F(200) - F_Q(200) , \quad (15)$$

whereas the construction from the Ca K images estimates this UV brightness component directly as

$$\Delta F_{\rm FAC}^{\rm MEAS}(200) = F_Q(200) \sum_{k=1}^{N_{\rm BINS}} \frac{N_k}{4N_{\rm PIX}} [(a + bI_{\rm Ca\,K}) - 1] \times (p + q\bar{\mu}_k + r\bar{\mu}_k^2 + s\bar{\mu}_k^3 + t\bar{\mu}_k^4) . \quad (16)$$

The adopted 200 nm quiet-Sun irradiance is 7.54 mW m^{-2} nm^{-1}, (see Fig. 2). The polynomial expression in $\bar{\mu}$ rep-

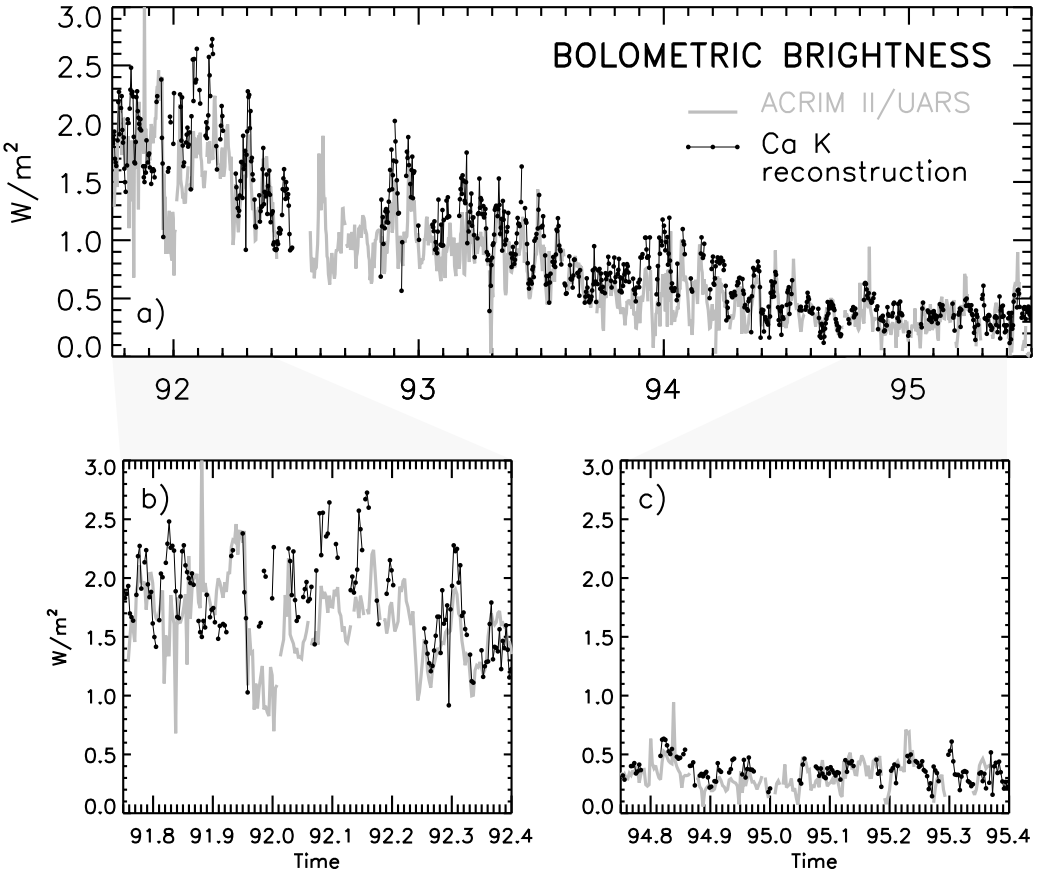

FIG. 9.—Bolometric brightness measured by ACRIM II (*gray line*), determined by subtracting the quiet-Sun and sunspot darkening from the radiometry compared with calculations of bolometric brightening attributable to magnetic sources that compose the residual histograms after removal of the background quiet Sun (*thin line with solid circles*). The full data record is shown in the upper panel (*a*), while the lower panels show selected portions of the record during high (*b*) and low (*c*) solar activity levels, respectively.

resents the 200 nm center-to-limb function in Figure 6*b*, and equation (16) assumes that the contrast of the 200 nm facular emission is independent of $\bar{\mu}$, consistent with Hersé's (1979) filtergram observations. Table 1 provides examples of the numerical values of the coefficients.

Figure 10 demonstrates that, like the bolometric radiation in Figure 9, the measured and constructed UV brightness components at 200 nm track each other closely throughout the solar cycle decline (see Fig. 10*a*) and over solar rotation in both maximum and minimum activity epochs (see Fig. 10*b*–10*c*). For the entire record of 614 mutual observations in Figure 10*a*, the correlation coefficient is 0.94 and the standard deviation is 0.05 mW m^{-2} nm^{-1}, which is less than 10% of the 0.6 mW m^{-2} nm^{-1} 200 nm brightness decrease shown in Fig. 10*a* for the cycle 22 decline.

5. DISCUSSION

5.1. *Facular versus Nonfacular Irradiance Brightening Components*

Extant facular and spot contrasts and center-to-limb functions combined with radiometrically determined quiet-Sun irradiances permit the construction of facular brightening that replicates quantitatively both the rotational modulation and the longer term solar cycle changes recorded independently by bolometric and UV space-based radiometers. The good agreement in Figures 9 and 10 between the measured total and UV facular brightening with constructions of enhanced emission in dense facular clumps and in the extended active network—identified by their Ca K surrogates—demontrates unambiguously that magnetic features are the predominant source of solar cycle irradiance brightening, based on data obtained during most of the declining phase of solar cycle 22.

Unlike empirical models of solar irradiance variability, in which regressions of facular proxies with the actual radiometric measurements determine the scalings needed to replicate the radiometry (see, e.g., Foukal & Lean 1988; Willson & Hudson 1991; Fröhlich 1994), the facular brightening calculations in Figures 9 and 10 are independent of the radiometry except for specification of the absolute value of the quiet-Sun irradiance [S_Q, $F_Q(200)$] to place the reconstructions on the same absolute irradiance scale as the measurements. Since over rotational timescales, the predominant cause of radiative output variability is the inhomogeneous distribution of magnetic sources on the disk, reproducing rotational modulation amplitudes requires proper specification of the product of the areas and contrasts of the bright facular clumps that are inhomogeneously distributed over the Sun's disk. Although there are large uncertainties in facular contrasts, which have not been observed at spatial resolutions that specifically match the BBSO Ca K images, the agreement of constructed and measured rotational modulation amplitudes evident in Figures 9 and 10 (*lower panels*) validates the adopted residual intensity contrast values (see, e.g., Fig. 8) for use with the BBSO Ca K images.

Mechanisms which are uniformly distributed in heliocentric longitude—i.e., global mechanisms—are not expected to cause significant rotational modulation, even

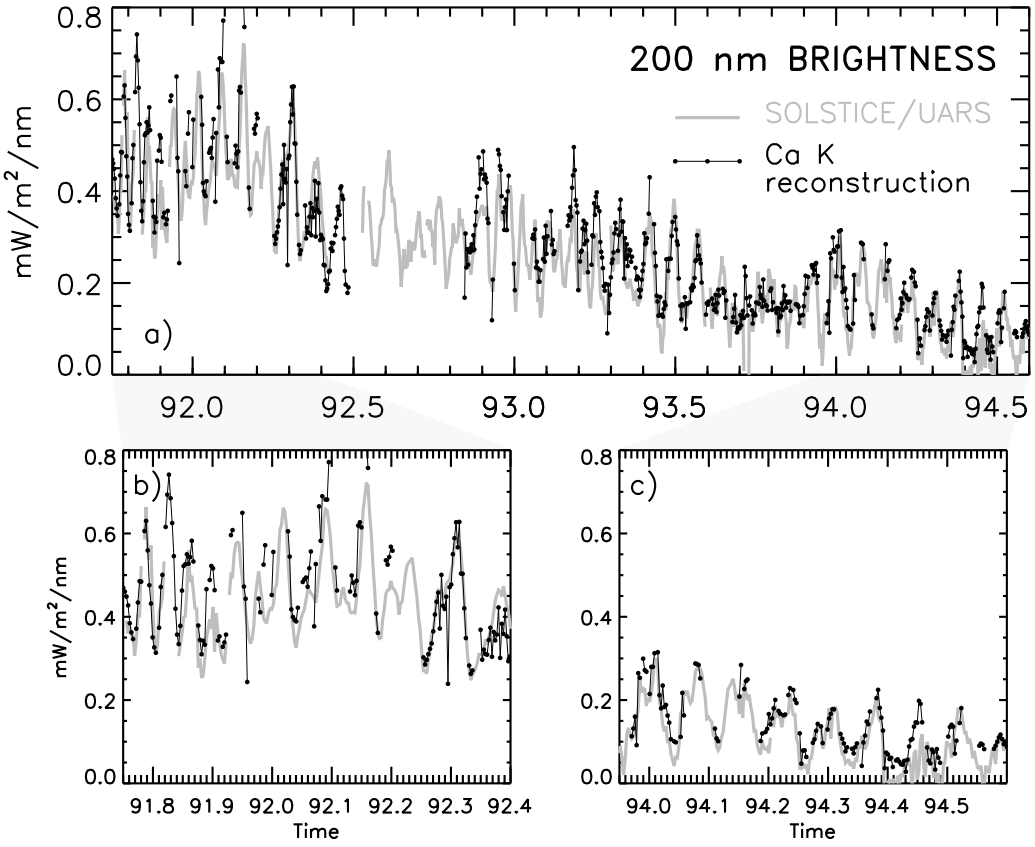

FIG. 10.—UV 200 nm brightness measured by SOLSTICE on *UARS* (*gray line*), determined by subtracting the quiet Sun from the radiometry compared with calculations of the 200 nm facular brightening attributable to magnetic sources that compose the residual histograms after removal of the background quiet Sun (*thin line with solid circles*). The full data record is shown in the upper panel (*a*) while the lower panels show selected portions of the record during high (*b*) and moderate to low (*c*) solar activity levels, respectively.

though they may contribute to longer term, solar cycle variability. That our constructed facular brightness changes replicate both the rotational modulation and the declining radiative output during solar cycle 22, which explains over 81% and 88% of the bolometric and 200 nm irradiance variations, respectively, obviates the need to postulate a missing brightness component. This would have been the case were the magnetic brightness sources insufficient to account for the longer term variations, even though they account fully for rotational modulation.

Recent analyses of full-disk magnetograms and He EW images likewise point to magnetic sources as the origin of solar irradiance variability (Harvey & White 1996), a result also inferred by Chapman et al. (1996) from a recent semi-empirical simulation of total irradiance variability using combinations of spatially resolved and global facular proxies. The ability to construct both the bolometric and the UV irradiance brightening at 200 nm with extant center-to-limb functions and contrasts further supports the conclusion that magnetic sources, rather than nonfacular mechanisms, control irradiance brightness. Whereas a nonfacular mechanism such as a small change in photospheric temperature may account for a 0.1% cycle in bolometric radiation, which emerges predominantly from the Sun's visible surface ($\log \tau = 1$ at 500 nm), UV radiation at 200 nm emerges from the middle photosphere ($\log \tau = 0.1$), about 250 km above the solar surface, and varies by an order of magnitude more than bolometric radiation. A more probable mechanism for these variations than a small surface temperature change is modulation by upward-extending magnetic flux tubes. This mechanism also accounts for the high correlation of bolometric and 200 nm radiation with each other with more variable chromospheric emissions, formed even higher in the Sun's atmosphere (Foukal & Lean 1990; Lean et al. 1995), as well as with various proxy records of the disk-integrated facular/plage emission—including the full-disk Ca K, He EW, and CN indices (Livingston et al. 1988). Solanki & Unruh (1997) reach similar conclusions from simulations of solar spectrum variability with models of the quiet and active solar atmosphere.

Our results point to the missing brightness component identified by Kuhn et al. (1988) as small scale facular emission unresolved in their limb measurements. Constructions of bolometric facular brightening are not greatly sensitive to assumptions about the center-to-limb dependence of bolometric facular contrast—the two scenarios in Figure 6 both permit simulations of radiometric brightness changes with correlation coefficients higher than 0.89. This is consistent with the finding of Foukal & Lean (1986) that measured bolometric brightness variations track the 200 nm irradiance (which lacks significant limb variation of the contrast) better than they track simulations of active region emission with significant limb brightening. Thus, the area of faculae on the solar disk rather than the center-to-limb brightening of their contrast appears to control bolometric brightness changes.

5.2. *Implications for Helioseismology*

Solar activity modulates the speed of pressure waves traveling beneath the Sun's surface. Detailed studies are beginning to identify perturbations of the Sun's internal *p*-mode oscillations by localized magnetic features such as sunspots and compact dense plages on its surface (Harvey 1995; Duvall et al. 1996). In postulating a global surface temperature change for the missing brightness component, Kuhn & Libbrecht (1991) and Kuhn & Stein (1966) have pointed out that a variability phenomenon extending over larger spatial scales also apparently contributes to *p*-mode frequency splittings during the solar cycle. Identifying small magnetic facular sources, dispersed widely over the Sun's surface as the missing brightness component of irradiance cycles, thereby implicates the role of the extended, dispersed active network faculae in helioseismic mode splittings that must be properly accounted for in order to invert the data to better probe the solar interior.

6. CONCLUSIONS

Our results indicate that magnetic sources cause the bolometric and UV 200 nm solar irradiance cycles. Using enhanced emission in full-disk Ca K filtergrams—after removing largescale instrumental effects and center-to-limb variations—as surrogates for these sources permits the construction of brightness changes during solar rotation, both at high and moderate to low levels of solar activity, and for most of the descending phase of solar cycle 22. These constructions use values of contrasts and center-to-limb functions that are consistent with observations of these quantities, and are independent of the direct radiometry aside from the adoption of the absolute irradiance scales.

Uncertainties exist in our constructed brightnesses because of the lack of rigorous radiometric control of the BBSO Ca K images (which were not intended for this purpose) and the lack of appropriate characterizations of the spatial characteristics of bolometric and UV facular, and active network on the solar disk. Uncertainties in the space-based radiometry itself also contribute; inconsistencies among different extant total irradiance data sets limit the ultimate inerpretation of the sources of the variability. Despite these limitations, the good agreement between the measured and constructed brightness changes, simultaneously for bolometric and 200 nm irradiance, during many solar rotations and most of the solar cycle decline, indicates that our conclusions are robust—that sufficient faculae are present on the Sun's disk during cycle maximum for their enhanced emission to explain the radiative output increase relative to cycle minimum.

This result, that global scale, nonfacular sources need not be invoked to account for the 11 yr bolometric and 200 nm irradiance cycles, does not address possible contributions by other sources of irradiance variability over longer timescales. Magnetic brightness sources used in our study are simply those identified in Ca K images as having brightnesses in excess of the background Sun, itself a mix of bright Ca emission in the network surrounding the supergranule cells, and the darker emission from the cell centers. Long-term changes in the fractional coverage and/or brightness of this quiet-Sun network, and possibly of the basal Ca K emission as well, are postulated as mechanisms for solar irradiance changes over multidecadal timescales, on which the 11 yr cycle is superimposed (White et al. 1992; Lean et al. 1992). The background Sun may change as a result of other mechanisms including changes in solar diameter and convective subsurface flows as well.

More precise determination and characterization of the facular sources of irradiance cycles require a new generation of ground-based observations to define properly the areas and contrasts of the bright emitting regions with mutually

consistent spatial resolution. The NSF RISE precision solar photometric telescope (PSPT) will contribute significantly to this goal. Whereas our results assumed facular contrasts and center-to-limb functions consistent with the available observations, future measurements by the PSPT should better specify the parameters needed to calculate brightness changes from solar images.

Also needed are improved observational specifications of the actual long-term irradiance changes over many solar cycles. While present solar monitoring has sufficient long-term precision to detect 11 yr irradiance cycles, uncertainties remain in the cycle amplitudes and year-to-year trends as a result of instrumental drifts on these timescales. Reducing these uncertainties will require continued deployment of multiple, overlapping radiometric instruments to monitor solar irradiance into the indefinite future. Present measurements by *UARS* (Willson 1994) and SOHO (Fröhlich et al. 1995, 1997) are contributing to this goal. Only a high-precision long-term database will permit exploration of the sources and mechanisms of climatically relevant centennial scale irradiance variations, if they occur.

A NASA SR&T grant supported the contributions of J. L. and J. C.; W. M. and A. J. acknowledge support by NASA MTPE. R. Willson provided the ACRIM data and participated in helpful discussions about the total irradiance database. G. Rottman and T. Woods produced the *UARS* SOLSTICE data. H. Warren helped with accessing the Ca K images. Frank Corprew and other personnel at the GSFC DAAC helped in accessing the *UARS* data. We greatly appreciate the numerous helpful and insightful comments on the manuscript by Peter Foukal.

REFERENCES

Allen, C. W. 1981, Astrophysical Quantities (3d ed.; London: Athlone)
Brandt, P. N., Stix, M., & Weinhardt, H. 1994, Sol. Phys., 152, 119
Chapman, G. A., Cookson, A. M., & Dobias, J. J. 1996, J. Geophys. Res., 101, 13541
Chapman, G. A., & Meyer, A. D. 1986, Sol. Phys., 103, 21
Chapman, G. A., & Sheeley, N. R., Jr. 1968, in IAU Symp. 35, Structure and Development of Solar Active Regions, ed. K. O. Kiepenheuer (Dordrecht: Reidel), 161
Cook, J W., Brueckner, G. E., & VanHoosier, M. E. 1980, J. Geophys. Res., 85, 2257
Cook, J. W., & Ewing, J. A. 1990, ApJ, 355, 719
DeLand, M. T., & Cebula, R. P. 1993, J. Geophys. Res., 98, 12809
de Toma, G., White, O. R., Knapp, B. G., Rottman, G. J., & Woods, T. N. 1997, J. Geophys. Res., 102, 2597
Duvall, T. L., D'Silva, S., Jefferies, S. M., Harvey, J. W., & Schou, J. 1996, Nature, 379, 235
Foukal, P. 1981, The Physics of Sunspots, ed. L. E., Cram & J. H. Thomas (Sacramento Peak Observatory), 391
Foukal, P., Harvey, K., & Hill, F. 1991, ApJ, 383, L89
Foukal, P., & Lean, J. 1986, ApJ, 302, 826
———. 1988, ApJ, 328, 347
———. 1990, Science, 247, 556
Fröhlich, C. 1994, in IAU Colloq. 143, The Sun as a Variable Star, ed. J. M. Pap, C. Fröhlich, H. S. Hudson, & S. K. Solanki (Cambridge: Cambridge Univ. Press), 28
Fröhlich, C., et al. 1997, Sol. Phys., 170, 1
Fröhlich, C., Pap, J. M., & Hudson, H. S. 1994, Sol.Phys., 152, 111
Fröhlich, C., et al. 1995, Sol. Phys., 162, 101
Harvey, J. 1995, Phys. Today, 1995 Oct., 32
Harvey, J. W., & Livingston, W. C. 1994, in IAU Symp. 154, Infrared Solar Physics, ed. D. M. Rabin, J. T. Jefferies, & C. Lindsey (Dordrecht: Norwell), 59
Harvey, K., & White, O. R. 1996, Sol. Phys. Res. Corp. Tech. Report 1996
Heath, D. F., & Schlesinger, B. M. 1986, J. Geophys. Res., 91, 8672
Hersé, M. 1979, Sol. Phys., 63, 35
Hickey, J. R., Alton, B. M., Kyle, H. L., & Hoyt, D. V. 1988, Space Sci. Rev., 48, 321
Hoyt, D. V., Kyle, H. L., Hickey, J. R., & Maschhoff, R. H. 1992, J. Geophys. Res., 97, 51
Hudson, H. S., Silva, S., Woodard, M., & Willson, R. C. 1982, Sol. Phys., 76, 211
Johannesson, A., Marquette, W. & Zirin, H. 1995, Sol. Phys., 161, 201
———. 1997, Sol. Phys., in press
Kuhn, J. R. 1989, ApJ, 339, L45
Kuhn, J. R., & Libbrecht, K. G. 1991, ApJ, 381, L35
Kuhn, J. R., Libbrecht, K. G., & Dicke, R. H. 1988, Science, 242, 908
Kuhn, J. R., & Stein, R. F. 1996, ApJ, 463, L117
Kyle, H. L., Hoyt, D. V., Hickey, J. R., Maschhoff, R. H., & Vallette, B. J. 1993, NASA Ref. Pub. 1316
Lawrence, J. K. 1988, Sol. Phys., 116, 17
Lawrence, J. K., Chapman, G A., & Walton, S. R. 1991, ApJ, 375, 771
Lean, J. 1988, Adv. Space Res., 8(7), 85
———. 1990, J. Geophys. Res., 95, 11933
Lean, J. 1991, Rev. Geophys., 29, 505
Lean, J. L., Mariska, J. T., Strong, K. T., Hudson, H. S., Acton, L. W., Rottman, G. J., Woods T. N., & Wilson, R. C. 1995, Geophys. Res. Lett., 22, 655
Lean, J., & Rind, D. 1996, Consequences, 2(1), 26
Lean, J. L., Rottman, G. J., Kyle, H. L., Woods, T. N., Hickey, J.R., & Puga, L. C. 1998, J. Geophys. Res., in press
Lean, J. L., Skumanich, A. & White, O. R. 1992, Geophys. Res. Lett., 19, 1591
Lean, J. L., White, O. R., Livingston, W. C., Heath, D. F., Donnelly, R. F., & Skumanich, A. 1982, J. Geophys. Res., 87, 10307
Lee III, R. B., Gibson, M. A., Wilson, R. S., & Thomas, S. 1995, J. Geophys. Res., 100, 1667
Libbrecht, K. G., & Kuhn, J. R. 1985, ApJ, 299, 1047
Livingston, W. C., Wallace, L., & White, O. R. 1988, Science, 240, 1765
Mecherikunnel, A. T. 1994, Sol. Phys., 155, 211
National Research Council. 1994, Solar Influences on Global Change (Washington, DC: Nat. Acad. Press)
National Research Council Space Studies Board. 1995, A Science Strategy for Space Physics (Washington, DC: Nat. Acad. Press)
National Space Weather Program. 1995, The Strategic Plan 1995 (FCM-P30-1995; Washington, DC)
Nishikawa, J. 1990, ApJ, 359, 235
Rottman, G. J. 1988, Adv. Space Res., 8(7), 53
Rottman, G. J., Woods, T. N., & Sparn, T. P. 1993, J. Geophys. Res., 98, 10667
Samain, D. 1979, A&A, 74, 225
Sheeley, N. R., Jr. 1967, ApJ, 147, 1106
Skumanich, A., Lean, J. L., White, O. R., & Livingston, W. C. 1984, ApJ, 282, 776
Skumanich, A., Smythe, C., & Frazier, E. N. 1975, ApJ, 200, 747
Solanki, S. K., & Unruh, Y. C. 1997, A&A, in press
Steinegger, M., Brandt, P. N., & Haupt, H. F. 1996, A&A, 310, 635
Vernazza, J. E., Avrett, E. H., & Loeser, R. 1976, ApJS, 30, 1
Vršnak, B., Placko, D., & Ruzdjak, V. 1991, Sol. Phys., 133, 205
White, O. R., & Livingston, W. C. 1981, ApJ, 249, 798
White, O. R., Skumanich, A., Lean, J., Livingston, W. C., & Keil, S. L. 1992, PASP, 104, 1139
Willson, R. C. 1979, Appl. Opt., 18, 179
———. 1982, J. Geophys. Res., 87, 4319
———. 1984, Space Sci. Rev., 38, 203
———. 1994, in IAU Colloq. 143, The Sun as a Variable Star, ed. J. M. Pap, C. Fröhlich, H. S. Hudson, & S. K. Solanki (Cambridge: Cambridge Univ. Press), 4
Willson, R. C., & Hudson, H. S. 1988, Nature, 332, 810
———. 1991, Nature, 351, 42
Willson, R. C., Gulkis, S., Janssen, M., Hudson, H. S., & Chapman, G. A. 1981, Science, 211, 700
Woods, T. N., Rottman, G. J., & Ucker, G. 1993, J. Geophys. Res., 98, 10679
Woods, T. N., et al. 1996, J. Geophys. Res., 101, 9541
Zirin, H., 1974, Sol. Phys., 38, 91